Three-dimensional Direct Numerical Simulations of Turbulent Lifted Non-premixed Hydrogen Jet Flames near Auto-ignition Limit

Seung Ook Kim[1], Jacqueline H. Chen[2], and Chun Sang Yoo[1,*]
[1]Department of Mechanical Engineering, Ulsan National Institute of Science and Technology, Ulsan 689-798, Republic of Korea.
[2]Combustion Research Facility, Sandia National Laboratories, Livermore, CA94551-0969, USA.

1 Introduction

The characteristics of turbulent lifted non-premixed jet flames under various coflow conditions have widely been investigated due to their relevance to practical applications such as diesel engines, gas turbine combustors, and commercial boilers. Moreover, the stabilization mechanisms of turbulent lifted jet flames are so complicated that it is still challenging to develop a predictive model, which is able to describe correctly every situation in turbulent combustion. Therefore, numerous studies of stabilization mechanisms of turbulent lifted jet flames in cold coflows have been conducted and various theories on the stabilization mechanisms have been proposed thus far [1]. Based on the premixedness of the mixture, they can be classified into premixed flame theory, non-premixed flamelet theory and edge flame theory. They can also be categorized into turbulent intensity theory and large eddy theory based on the local flow effect. In many practical applications, however, ambient air around fuel jet is hot enough to induce auto-ignition of fuel/air mixture upstream of the flamebase. As such, auto-ignition has been found as the primary stabilization mechanism of turbulent lifted flames in hot vitiated coflows. Previous 3-D direct numerical simulations (DNSs) of hydrogen [2] and ethylene [3] jet flames in highly-heated coflows revealed that turbulent lifted jet flames are stabilized primarily by the auto-ignition of fuel-lean mixtures supported by the hot coflow temperature exceeding the auto-ignition limit and are also determined by the balance between the local axial velocity and consecutive auto-ignition events occurring in hot fuel-lean mixtures.

However, the stabilization mechanism of turbulent lifted jet flames in mildly-heated coflows of which temperature is near auto-ignition limit has not been extensively investigated, even though the overall characteristics of such flames were reported in experimental studies [4,5]. From these experiments, it was found that the lift-off height correlates well with the inlet jet velocity based both on the premixed flame theory and the large eddy theory regardless of the inlet temperatures. For the large eddy theory, however, the thermal diffusivity evaluated at the inlet temperature rather than at the burnt gas temperature is adopted to obtain a proper correlation. In this study, therefore, three 3-D DNSs of turbulent lifted hydrogen/air jet flames in heated coflows near auto-ignition limit are performed to examine the stabilization mechanisms and flame structure of turbulent lifted jet flames.

2 Problem configuration

Three different DNSs of spatially-developing turbulent lifted jet flames were performed in a 3-D slot-burner configuration. Fuel issues from a central jet, which consists of 65% hydrogen and 35% nitrogen by volume at an inlet temperature of $T_j = 400$ K. The central jet is surrounded on either side by co-flowing heated air streams at three different temperatures of $T_c = 750$ (Case L), 850 (Case M), and 950 K (Case H) and atmospheric pressure. The fuel jet and coflow velocities are specified as $U_j =$ 240 m/s and $U_c = 2$ m/s, respectively. The fuel jet width, H, is 2 mm such that the jet Reynolds number, $Re_j (= U_j H/\nu)$, is approximately 8000. The computational domain is $15H \times 20H \times 3H$ in the streamwise, x, transverse, y, and spanwise, z, directions with $2000 \times 1600 \times 400$ grid points. A uniform

*Correspondence to: csyoo@unist.ac.kr

grid spacing of 15 μm is used in the *x*- and *z*-directions, while an algebraically stretched mesh is used in the *y*-direction as in [3].

The compressible Navier-Stokes, species continuity, and total energy equations were solved using the Sandia DNS code, S3D, with a 4th-order Runge-Kutta method for time integration and an 8th-order central differencing scheme for spatial discretization. A detailed hydrogen/air kinetic mechanism was adopted for DNSs [6]. Improved nonreflecting inflow/outflow boundary conditions [7,8] were used in the *x*- and *y*-directions and periodic boundary conditions were applied in the homogeneous *z*-direction. Based on the fuel jet velocity and the streamwise domain length, a flow-through time, $\tau_j = L_x/U_j$, is 0.125 ms. To obtain a stationary lifted flame while reducing computational cost, a simulation with a grid resolution of 40 μm was first performed until the flame attained statistical stationarity. The solutions from the simulation were then mapped onto a finer grid of 15 μm and used as an initial condition for the fully resolved simulations. The solutions were then advanced at a constant time-step of 5 ns through $4.0\tau_j$. The DNSs were performed on the Cray XT5/XK7 at Oak Ridge National Laboratories and each DNS required approximately 2.5 million CPU-hours. Note that the steady lift-off heights are found to be approximately $\bar{h}_H/H = 2.4$, $\bar{h}_M/H = 4.0$, and $\bar{h}_L/H = 5.3$. Figure 1 shows 3-D volume-rendering of the mass fraction of OH and HO_2 at t/τ_j = 2.0.

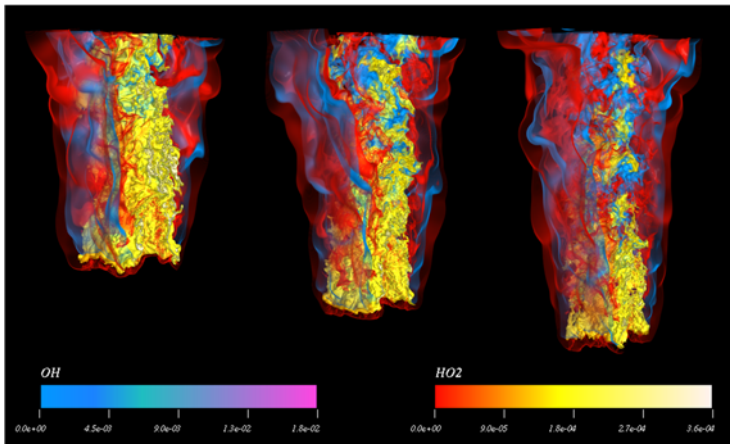

Figure 1. 3-D volume rendering of OH and HO_2 mass fractions of turbulent lifted hydrogen jet flames for Cases L, M, and H (from left to right)

3 Overall Flame Characteristics

To understand the overall characteristics of turbulent lifted jet flames, cross-stream conditional Favre mean of a variable φ, $\langle\varphi|\eta\rangle$, is adopted, which is defined by:

$$\langle\varphi|\eta\rangle = \iiint(\rho(\mathbf{x},t)\varphi(\mathbf{x},t)|\xi=\eta)dydzdt \Big/ \iiint(\rho(\mathbf{x},t)|\xi=\eta)dydzdt, \quad (1)$$

where η is the sample space of the mixture fraction, ξ. Figure 2 shows the conditional Favre means of temperature, $\langle T|\eta\rangle$, and heat release rate, $\langle\dot{q}|\eta\rangle$, along the streamwise direction. Several points are to be noted from the figure. First, $\langle\dot{q}|\eta\rangle$ increases first in fuel-lean mixtures and the maximum $\langle\dot{q}|\eta\rangle$ occurs approximately at one jet width downstream of the lift-off height in all cases. It is also observed that the peak $\langle\dot{q}|\eta\rangle$ occurs at stoichiometric to slightly rich conditions within a jet width downstream of the lift-off height and rapidly decreases further downstream. This result implies that for all cases, vigorous reaction occurs within one jet width downstream of the lift-off height. Second, in Case H, relatively large $\langle\dot{q}|\eta\rangle$ occurs in fuel-lean mixture at the lift-off height compared to Case L, implying that high T_c in Case H induces greater heat release at fuel-lean mixtures. Third, in all cases, two peaks in $\langle\dot{q}|\eta\rangle$ form further downstream of the flame base, one centered near the stoichiometric and the other centered in fuel-rich mixtures, consistent with the result of our previous DNS study [2]. In addition, for Case L, there is no heat release at large mixture fraction ($\eta \geq 0.7$) even far downstream of the liftoff height and

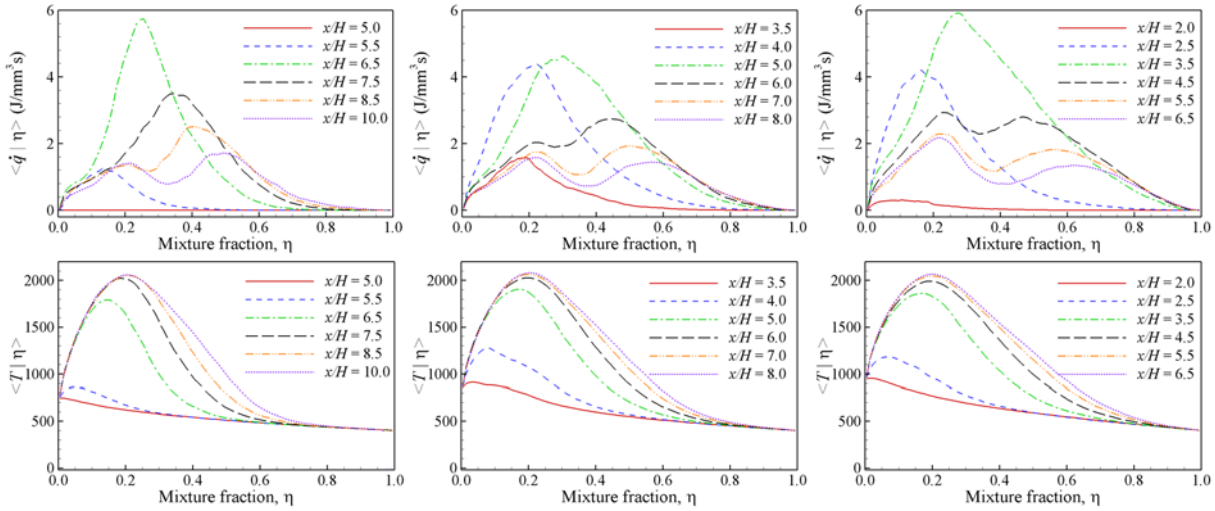

Figure 2. Conditional Favre mean of heat release rate (top) and temperature (bottom) for Cases L, M, and H (from left to right)

as such, $\langle T|\eta\rangle$ exhibits the pure mixing limit. For Cases M and H, however, $\langle \dot{q}|\eta\rangle$ has significant values even at $\eta \geq 0.7$ downstream of the flame base. As a result, $\langle T|\eta\rangle$ increases significantly beyond the pure mixing limit values. The results imply that combustion at rich mixtures account for significant amount of heat release, comparable to that from lean to stoichiometric flames.

To further identify the characteristics of the stabilization mechanism, $\langle Da|\eta\rangle$ along the streamwise direction is shown in Fig. 4 for the two cases. The Damköhler number, Da, is defined as [2,3]: $Da = \dot{\omega}_k/|-\nabla\cdot(\rho Y_k \boldsymbol{V}_k)|$, where $\boldsymbol{V}_k$ and $\dot{\omega}_k$ denote a diffusive velocity vector and a net production rate of species k, respectively. In this study, H_2O is adopted for the Damköhler number analysis. Since Da is defined as the ratio of species reaction term to diffusion, it provides a measure of the local progress of ignition. Therefore, large values of $Da \sim O(\gg 1)$ indicates significant increase of heat and radicals due to ignition.

It is readily observed from the figure that $\langle Da|\eta\rangle$ exhibits significantly different behavior near the flamebase, which indicates that the three lifted flames may be stabilized by different mechanisms. In Case H, $\langle Da|\eta\rangle$ exhibits large value ($\gg 1$) at fuel-lean mixtures near and upstream of the flame base. In addition, the variance of Da (not shown) is considerably larger than the conditional mean value. This result suggests that the local Da can be significantly larger than unity, and hence, auto-ignition can be the main source of stabilization of the lifted flame in Case H. In Case L, however, $\langle Da|\eta\rangle$ is nearly zero upstream of the flamebase and exhibits $O(\sim 1)$ at lean mixtures near the flamebase. In addition, the variance of Da is relatively small compared to that in Case H, suggesting that for Case L, the reaction and diffusion terms balance each other and as such, flame propagation is the stabilization mechanism of the lifted flame. For Case M, $\langle Da|\eta\rangle$ has much larger values near the flamebase compared to that of Case L but smaller than that for Case H such that it is not straightforward to determine which mechanism stabilizes the lifted flame.

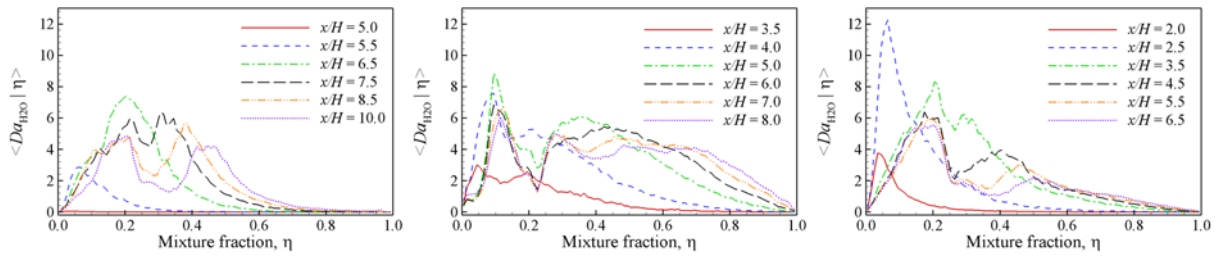

Figure 4. Conditional Favre means of *Da* at different axial locations for Cases L, M, and H (from left to right)

4 Chemical Explosive Mode Analysis (CEMA)

Chemical explosive mode analysis (CEMA) is adopted to further identify the characteristics of the lifted flamebases [9~11]. CEMA is briefly introduced here and for more details of it, refer to [9,10]. The differential equations of a typical reacting flow can be described in discretized form as:

$$\frac{D\mathbf{y}}{Dt} = \mathbf{g}(\mathbf{y}) = \boldsymbol{\omega}(\mathbf{y}) + \mathbf{s}(\mathbf{y}), \tag{3}$$

where D/Dt is the material derivative, which can be replaced by d/dt in the Lagrangian coordinate, and $\mathbf{y}$ represents the solution vector of species concentrations and temperature. The chemical source term is denoted as $\boldsymbol{\omega}$, while all non-chemical source terms such as diffusion in flames and homogeneous mixing term in stirred reactors are represented by $\mathbf{s}$.

The Jacobian matrix of the chemical source term, $\mathbf{J}_{\boldsymbol{\omega}}$ $(\equiv \partial\boldsymbol{\omega}/\partial\mathbf{y})$, can fully describe the local chemical information such that a chemical mode can be defined as an eigenmode of $\mathbf{J}_{\boldsymbol{\omega}}$, which is associated with an eigenvalue and a corresponding pair of the left and right eigenvectors ($\mathbf{a}_e$ and $\mathbf{b}_e$). CEM is defined as a chemical mode of which real part of the eigenvalue, λ_e, is positive. CEM represents the reciprocal chemical time scale of a local mixture and as such, the existence of CEM implies that the corresponding mixture is explosive in nature. It is, therefore, apt to auto-ignite when the mixture resides in a lossless environment with negligible $\mathbf{s}$ in Eq. (3). However, a mixture exhibiting CEM does not necessarily lead to thermal run-away if the mixture significantly loses heat and radicals. Therefore, CEM is an intrinsic characteristic of ignitable mixtures.

In nonpremixed turbulent flames, the loss of heat and radicals can be characterized by the mixing or scalar dissipation rate, χ, which is defined by $\chi = 2D|\nabla\xi|^2$, where D is local thermal diffusivity. The competition between the CEMs and the losses can approximately be quantified by a Damköhler number defined by $Da_c = \lambda_e \cdot \chi^{-1}$. Note that mixture with $Da_c \gg 1$ indicates a dominant CEM which will be likely to result in actual ignition; otherwise ignition may be suppressed by the losses.

Figure 5 shows isocontour of Da_c in logscale for the cases. Note that a large positive Da_c in red indicates that the CEM dominates the mixing process such that the mixture is auto-igniting. A large negative Da_c in blue, however, indicates fast reacting post-ignition mixture such that its overall reaction progress can be limited by the slower local transport process. As such, the dark blue regions in Fig. 5 contain diffusion flame kernels. It is also readily observed that for Case H, there exist two strips of auto-igniting mixtures (red) upstream of the flamebase, leading to ignited mixtures (blue). This result verifies that the stabilization mechanism of Case H is auto-ignition. In Cases L and M, however, large positive Da_c occurs only at narrow regions right upstream of the flamebase, which corrspond to the preheated zone of a premixed flame. This result verifies that turbulent lifted flames for Cases L and M are mainly stabilized by flame propagation whereas the stabiliztion of the lifted flame for Case H is primarily attributed to auto-ignition of fuel-lean mixtures upstream of the flamebase.

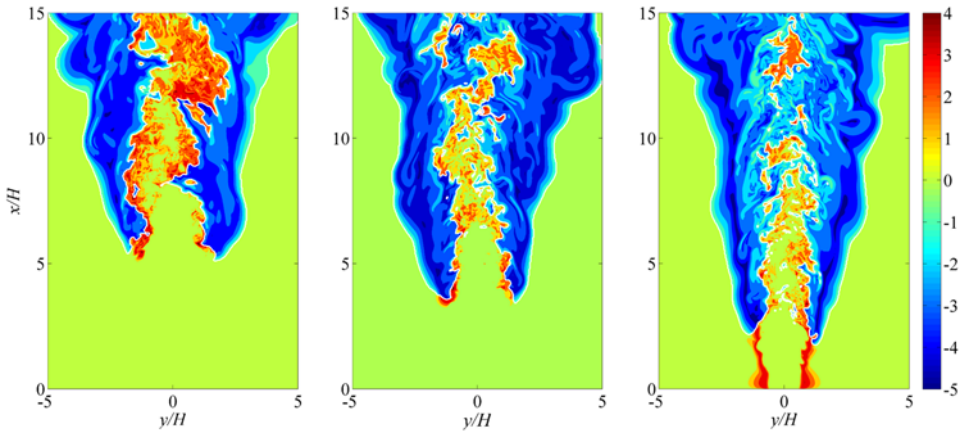

Figure 5. Isocontours of sign(λ_e)×log$_{10}$(max(1,|Da_c|)) for Cases L, M, and H (from left to right). White lines denote the flamebase with $Da_c = 1$.

The physicochemical characteristics of the flames are further investigated using the explosion index (EI) and participation index (PI), which represent the contribution of variables and reactions to CEM, respectively. The EI and PI vectors are defined as [9,10]:

$$\mathbf{EI} = \frac{|\mathbf{a}_e \otimes \mathbf{b}_e^T|}{sum(|\mathbf{a}_e \otimes \mathbf{b}_e^T|)},$$

$$\mathbf{PI} = \frac{|\mathbf{b}_e \cdot \mathbf{S} \otimes \mathbf{R}|}{sum(|(\mathbf{b}_e \cdot \mathbf{S}) \otimes \mathbf{R}|)},$$

where **S** and **R** represent the stoichiometric coefficient matrix and the vector of the net rates for reactions, respectively and the symbol ⊗ represents the element-wise multiplication of two vectors.

Figure 6 shows EI-weighted color-mixing contours of important variables to the CEM. In addition, the variables and reactions with large EI and PI values at ten different locations are listed in Table 1. For all cases, temperture is found to be the most important variable right upstream of the flamebase. This is because temperaure becomes critical to a CEM in the preheated zone of premixed flame in Cases L and M, and in the thermal ignition layer upstream of the flamebase in Case H. Unlike Cases L and M, however, O and OH radicals are found to be important in the auto-igniting layers that can stabilize the lifted flame in Case H. In addition, two important reactions that control the auto-igniting layer are R1 ($H + O_2 = O + OH$) and R9 ($H + O_2 + M = HO_2 + M$). This is because R1 and R9 are two competing reactions determining the 2nd explosion limit of H_2/O_2 mixture. It is also of interest to note that even in the preheated zone of Case L & M, and thermal ignition layer of Case H where temperature governs the CEM, R1 and R9 are also found to be the two most important reactions to the CEM. It is primarily because R9 is one of the major heat release reactions and R1 is the major endothermic reaction in both premixed and non-premixed H_2/air flames.

In the lean mixtures of the lifted flames, H_2 becomes important to the CEM; however, in the rich mixtures of the flames, H becomes critical to rich premixed flame. From PI analysis (see Table 1), it is readily observed that in the lean mixures (Point 1), two major heat release reactions, R3 ($OH + H_2 = H_2O + H$) and R9 are identified as the most important reactions to the CEM. In the rich mixtures (Points 3 and 5), however, R8 ($H + OH + M = H_2O + M$) and R9 are found critical to the CEM. It is also of importance to note that near the stoichiometric mixtures (Point 2), O and H are important EI species and R9 & R8 are the critical PI reactions.

5 Conclusions

The characteristics of stabilization mechanism and flame structure of turbulent lifted hydrogen jet flames in heated coflow at three temperatures of 750, 850 and 950 K near auto-ignition limit were investigated using direct numerical simulations with a detailed hydrogen oxidation mechanism. Overall flame structure and chemical explosive mode analyses revealed that auto-ignition is the main stabilization mechanism of the lifted jet flame for Case H; however, for Cases L & M, normal flame propagation is found to be the main stabilization mechanism rather than auto-ignition. EI and PI analyses identified important variables and reactions for the lifted hydrogen jet flames. For all cases, T and H_2 are important variables in the preheated zone and thermal ignition layer upstream of the flamebase, where R1 and R9 are found the most importance reactions to the CEM. This is not only because they are two competing reactions determining the 2nd explosion limit of H_2/air mixture but also because they are the major endothermic and exothermic reactions in the premixed and non-premixed H_2/air flames.

Acknowledgement

This work was supported by the National Research Foundation of Korea (NRF) grant funded by the Korea government (MSIP) (No. 2015R1A2A2A01007378).

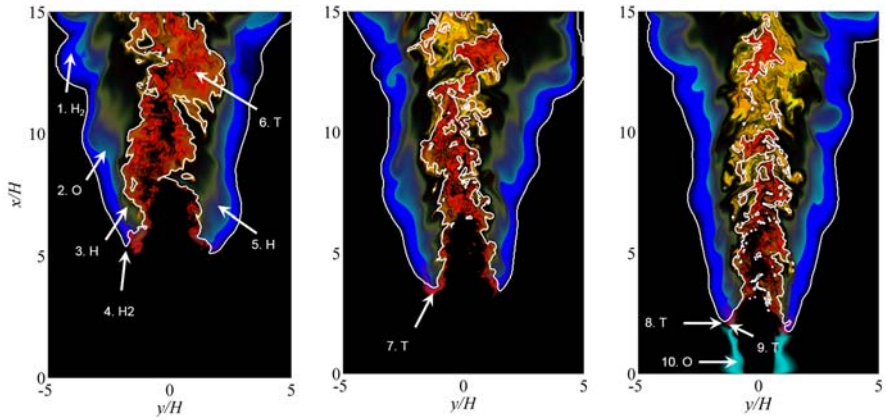

Figure 5. EI-weighted color-mixing contours of temperature (red), H_2 (blue), H (green), O (cyan), and O_2 (yellow) for Cases L, M, and H. White lines denote the flamebase with $Da_c = 1$.

Table 1: EI and PI values at selected points

Point	**Location**	**EI** (value, variables)	**PI** (value, reaction)
1	x = –4.03H y = 13.18H	0.99, H_2	0.49, R3: OH + H_2 = H_2O + H 0.13, R9: H + O_2 + M = HO_2 + M
2	x = –2.61H y = 9.24H	0.40, O 0.27, H	0.69, R9: H + O_2 + M = HO_2 + M 0.14, R8: H + OH + M = H_2O + M
3	x = –1.71H y = 6.90H	0.56, H 0.19, O_2	0.70, R8: H + OH + M = H_2O + M
4	x = –1.8H y = 5.34H	0.49, H_2 0.47, T	0.49, R1: H + O_2 = O + OH 0.43, R9: H + O_2+ M = HO_2 + M
5	x = 2.01H y = 6.96H	0.37, H 0.28, H_2	0.67, R8: H + OH + M = H_2O + M 0.18, R9: H + O_2 + M = HO_2 + M
6	x = 1.05H y = 12.48H	0.84, T	0.34, R11: HO_2 + H = OH + OH 0.19, R3: H_2 + OH = H_2O + OH
7	x = –1.26H y = 3.33H	0.87, T	0.43, R9: H + O_2 + M = HO_2 + M 0.38, R1: H + O_2 = O + OH
8	x = –1.47H y = 2.13H	0.53, T 0.41, H_2	0.50, R9: H + O_2 + M = HO_2 + M 0.50, R1: H + O_2 = O + OH
9	x = –1.23H y = 2.04H	0.69, T 0.15, H_2	0.48, R9: H + O_2 + M = HO_2 + M 0.47, R1: H + O_2 = O + OH
10	x = –0.93H y = 0.54H	0.80, O 0.18, OH	0.40, R1: H + O_2 = O + OH 0.40, R9: H + O_2 + M = HO_2 + M

References

[1] K. M. Lyons, Prog. Energy Combust. Sci. 33 (2007) 211–231.
[2] C. S. Yoo, R. Sankaran, J. H. Chen, *J. Fluid Mech.* 640 (2009) 453–481.
[3] C. S. Yoo, E. S. Richardson, R. Sankaran, J. H. Chen, *Proc. Combust. Inst.* 33 (2011) 1619–1627.
[4] K. N. Kim, S. H. Won, S. H. Chung, *Proc. Combust. Inst.* 31 (2007) 1591–1598.
[5] S. H. Chung, *Proc. Combust. Inst.* 32 (2007) 877–892.
[6] J. Li, Z. Zhao, A. Kazakov, F. L. Dryer, *Int. J. Chem. Kinet*. 36 (2004) 566–575.
[7] C. S. Yoo, Y. Wang, A. Trouvé, H. G. Im, *Combust. Theory Modelling* 9 (2005) 617–646.
[8] C. S. Yoo, H. G. Im, *Combust. Theory Modelling* 11 (2007) 259–286.
[9] T. Lu, C. S. Yoo, J. H. Chen, C. K. Law, *J. Fluid Mech*. 652 (2010) 45–64.
[10] Z. Luo, C. S. Yoo, E. S. Richardson, J. H. Chen, C. K. Law, *Combust. Flame* 159 (2012) 265–274.
[11] R. Shan, C. S. Yoo, J. H. Chen, T. Lu, *Combust. Flame* 159 (2012) 3119–3127.